ORGANOMETALLICS
Article

Organometallics **2010,** *29,* 795–800 795
DOI: 10.1021/om900676m

Periodic and Molecular Modeling Study of Donor−Acceptor Interactions in (dbbpy)Pt(tdt)·TENF and [Pt(dbbpy)(tdt)]$_2$·TENF

Thomas R. Cundari,*[,†] Bhaskar Chilukuri,[†] Joshua M. Hudson,[†] Christian Minot,[‡] Mohammad A. Omary,[†] and Hassan Rabaâ[§]

[†]*Department of Chemistry, Center for Advanced Scientific Computing and Modeling (CASCaM), University of North Texas, Box 305070, Denton, Texas 76203-5070,* [‡]*Laboratoire de Chimie Théorique, UMR 7616 UPMC/CNRS, Université Pierre et Marie Curie, 75252 Paris 5, France, and* [§]*Department of Chemistry, ESCTM, Ibn Tofail University, P.O. Box 133, Kenitra, 14000, Morocco*

Received July 30, 2009

Supramolecular stacked materials (dbbpy)Pt(tdt)·TENF and [Pt(dbbpy)(tdt)]$_2$·TENF are built from (dbbpy)Pt(tdt) donors (D) with TENF acceptors (A) (TENF = 2,4,5,7-tetranitro-9-fluorenone; dbbpy = 4,4′-di-*tert*-butyl-2,2′-bipyridine; tdt = 3,4-toluenedithiolate). Simulations using extended Hückel tight binding (EHTB) and plane-wave DFT methods are performed. From EHTB analysis, the density of states (DOS) of D/A and DD/A stacks exhibit metallic behavior with a large contribution from TENF π in the valence band mixed with more significant Pt character in the D/A than in the DD/A stacks. DOS modification and charge transfer are estimated via analysis of the stacking sequences. Theoretical results from plane-wave DFT calculations give evidence of semimetallic behavior for the D/A material (gap < 0.1 eV) and metallic behavior for DD/A. Fragment analysis was performed, and similarities and differences between EHTB and DFT were noted. Molecular DFT computations suggest that the close ($\sim$3.6 Å) D−A distances are sufficient to allow some intermolecular donor-to-acceptor charge transfer and higher interaction energy in DD/A than in D/A units, consistent with the periodic calculations for the solid-state stacks. Calculation of metric data via modeling of a (dbbpy)Pt(tdt)·TENF cluster as well as neutral, cationic, and anionic TENF are used to assess the fractional charge on TENF and hence the degree of D → A charge transfer.

Introduction

Dunbar, Omary, and co-workers have studied novel supramolecular stacks containing inorganic donors of the formula (dbbpy)M(dmid) (M = Pt, Pd; dbbpy = 4,4′-di-*tert*-butyl-2,2′-bipyridine; dmid = 2-oxo-1,3-dithiole-4,5-dithiolate) with different nitrile acceptors such as TCNQ (TCNQ = 7,7,8,8-tetracyanoquinodimethane).[1] These materials display interesting optoelectronic properties in solution and in the solid state: e.g., as photosensitizing dyes for solar cells based on wide band gap semiconductors.[1,2] Omary and co-workers[1b,c] have synthesized new supramolecular systems containing (dbbpy)Pt(tdt) (tdt = 3,4-toluenedithiolate) and the organic acceptor TENF (TENF = 2,4,5,7-tetranitro-9-flourenone) (Scheme 1). The (dbbpy)Pt(tdt)·TENF supramolecular system has been characterized by X-ray crystallography, cyclic voltammetry, and IR, UV−Vis−near-IR electronic absorption, diffuse reflectance, and NMR spectroscopies.[1b,c]

The stacking pattern of donors (D) and acceptors (A) and their relative orientation in the solid state impact the conductivity of such materials, yielding metallic, insulating, or semiconducting properties.[1−4] Interestingly, by changing the crystal growth conditions, the stacking in the aforementioned materials varies in the ratio of donor to acceptor molecules. For (dbbpy)Pt(tdt) and TENF, crystallography reveals both a 1:1 (D/A) stacking pattern of the donor and acceptor molecules (Figure 1), as well as a 2:1 (DD/A) pattern (Figure 2).[1b,c] Both patterns crystallize in the $P2_1/n$ space group. The crystal structure of (dbbpy)Pt(tdt)·TENF has a linear chain structure with D/A stacking and close D:A contacts of 3.49 Å. The DD/A material has D:A and D:D distances of 3.34 and 3.45 Å, respectively. In the latter, the TENF molecule is sandwiched between two donor molecules (Figure 2).

This paper reports molecular calculations of Pt-based donor−acceptor materials. The electronic structure and charge transfer

*To whom correspondence should be addressed. E-mail: t@unt.edu. Tel: 940-369-7753. Fax: 940-565-4318.

(1) (a) Smucker, B. W.; Hudson, J. M.; Omary, M. A.; Dunbar, K. R. *Inorg. Chem.* **2003**, *42*, 4714. (b) Hudson, J. M. *Ph.D. Dissertation*, University of North Texas, Denton, TX, 2007. (c) Hudson, J. M.; Reinheimer, E. W.; McDougald, R. N., Jr.; Rabaa, H.; Bacsa, J.; Dunbar, K. R.; Wang, X.; Omary, M. A. Synthesis and Characterization of Black Absorbers Based on Charge Transfer Complexes with a Pt(Bipyridine)(Dithiolate) Donor and Nitrofluorenone Acceptors, submitted for publication. (d) Olmstead, M. M.; Jiang, F.; Attar, S.; Balch, A. L. *J. Am. Chem. Soc.* **2001**, *123*, 3260. (e) Ishibashi, S.; Hasimoto, T.; Kohyama, T.; Terakura, K. *Phys. Rev. B* **2004**, *69*, 155111.

(2) (a) Rand, B. P.; Xue, J.; Uchida, S.; Forrest, S. R. *J. Appl. Phys.* **2005**, *98*, 124902. (b) Xue, J.; Rand, B. P.; Uchida, S.; Forrest, S. R. *J. Appl. Phys.* **2005**, *98*, 124903. (c) Shirota, Y.; Kageyama, H. *Chem. Rev.* **2007**, *107*, 953. (d) Coropceanu, V.; Cornil, J.; Da Silva Filho, D. A.; Olivier, R.; Brédas, S. J. *Chem. Rev.* **2007**, *107*, 926. (e) Walzer, K.; Maennig, B.; Pfeiffer, M.; Leo, K. *Chem. Rev.* **2007**, *107*, 1233.

(3) (a) Shaik, S. S. *J. Am. Chem. Soc.* **1982**, *104*, 5328. (b) McConnell, H. M.; Hoffman, B. M.; Metzger, R. M. *Proc. Natl. Acad. Sci. U.S.A.* **1965**, *53*, 46. (c) Miller, J. S.; Epstein, A. J. *J. Am. Chem. Soc.* **1987**, *109*, 3850.

(4) (a) Islam, A.; Sugihara, H.; Hara, K.; Singh, L. P.; Katoh, R.; Yanagida, M.; Takahashi, Y.; Murata, S.; Arakawa, H. *New J. Chem.* **2000**, *24*, 343. (b) Rabaâ, H.; Cundari, T. R.; Omary, M. A. *Can. J. Chem.* **2009**, *87*, 775. (c) Chen, W.-H.; Reinheimer, E. W.; Dunbar, K. R.; Omary, M. A. *Inorg. Chem.* **2006**, *45*, 2770.

Published on Web 01/15/2010

Scheme 1. Chemical Structure of (dbbpy)Pt(tdt) Donor (D, Left) and TENF Acceptor (A, Right)

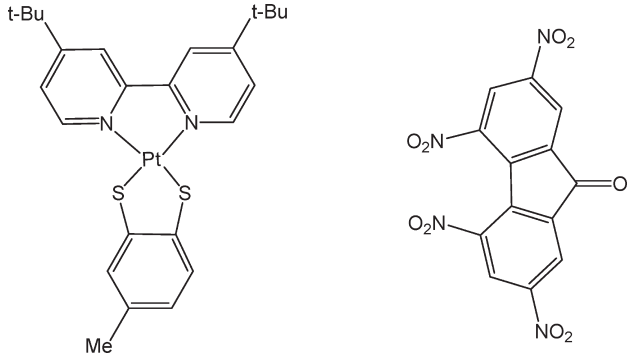

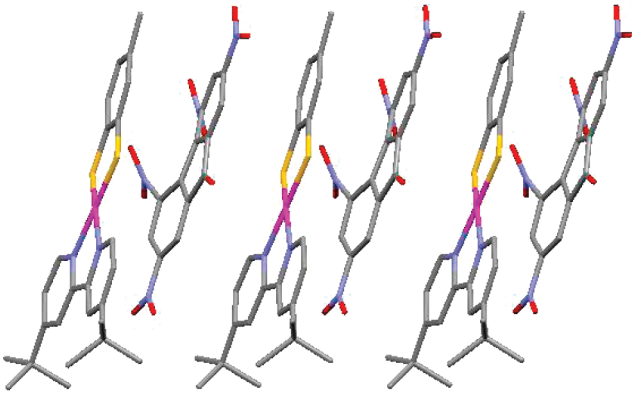

Figure 1. D/A stacks of (dbbpy)Pt(tdt)·TENF from the experimental crystal structure.[1b,c] Legend: Pt, magenta; C, gray; N, blue; O, red; S, yellow.

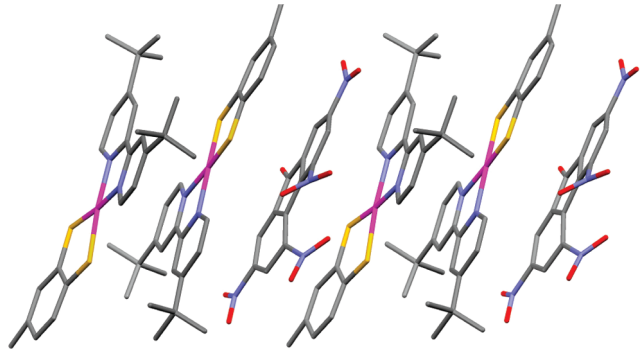

Figure 2. Crystallographic structure for $[Pt(dbbpy)(tdt)]_2$·TENF showing DD/A stacking.[1b,c] Legend: Pt, magenta; C, gray; N, blue; O, red; S, yellow.

properties of D/A and DD/A stacks are analyzed: viz. (dbbpy)-Pt(tdt)·TENF and $[Pt(dbbpy)(tdt)]_2$·TENF, respectively. We focused our research on the structural and electronic parameters of these stacks, the fractional charge on TENF, and the implications of these for D to A charge transfer.

(5) (a) Hoffmann, R.; Lipscomb, W. N. *J. Chem. Phys.* **1962**, *36*, 2179. (b) Hoffmann, R.; Lipscomb, W. N. *J. Chem. Phys.* **1962**, *36*, 3489. (c) Hoffmann, R.; Lipscomb, W. N. *J. Chem. Phys.* **1963**, *37*, 590. (d) Hoffmann, R. *J. Chem. Phys.* **1963**, *39*, 1397. (e) Hoffmann, R. *Solids and Surfaces: A Chemist's View of Bonding in Extended Structures*; Wiley-VCH: New York, 1988. (f) Whangbo, M.-H.; Hoffmann, R. *J. Am. Chem. Soc.* **1978**, *100*, 6093. (g) Whangbo, M.-H.; Hoffmann, R.; Woodward, B. *Proc. R. Soc. London, Ser. A* **1979**, *366*, 23.

Computational Methods

Given the large unit cells of the periodic systems studied in this research, most solid-state simulations are performed within the framework of the extended Hückel tight binding (EHTB) method[5] for which standard parameters are used in the YAeHMOP[6] package. This method has been widely used in simulation of the bonding and structure of extended chemical systems.[5] In this research, EHTB is compared with more expensive plane-wave DFT calculations when deemed prudent. Given the difficulties in predicting band gaps with standard DFT approaches,[7] EHTB calculations remain valuable in evaluating salient electronic structural features of materials for which crystal structures are known. EHTB calculations have also proven helpful in identifying the various atomic/fragment contributions to bands in the vicinity of the Fermi level.[8] The off-diagonal elements of the EHTB Hamiltonian are evaluated with the Wolfsberg−Helmholtz formula. Numerical integrations over the symmetry-unique section of the Brillouin zone of the three-dimensional structure of [(dbbpy)-$Pt(tdt)]_{1,2}$·TENF were performed using a set of 64 k-points.[5,6]

Some solid-state calculations were carried out using the VASP (Vienna ab initio simulation program) code.[9] Density functional theory within the PAW (projector-augmented wave) method[10] and the generalized gradient approximation (GGA) functional of Perdew, Burke, and Ernzerhof (PBE)[11] was employed. The electronic wave functions were sampled on a $1 \times 3 \times 1$ k-mesh in the irreducible Brillouin zone (BZ) using the Monkhorst and Pack method.[12] The cutoff energy of the wave functions was 400 eV. Convergence of the total energy with the k-mesh in the Brillouin zones and the plane wave cutoff energy was checked. Ultrasoft pseudopotentials were used together with plane wave basis sets.[13]

The Gaussian 03 package is used for the molecular density functional calculations described herein.[14] Stevens' effective core potentials and valence basis sets[15] (augmented with a set of d polarization functions for main-group atoms) are employed in conjunction with the B3LYP hybrid functional.[16] All molecular geometries are optimized with restricted Kohn−Sham methods for singlets and unrestricted Kohn−Sham methods for higher multiplicities. Vibrational frequencies are calculated at all stationary points to characterize them as minima (i.e., no imaginary frequencies).

Results

1. Solid-State Electronic Structure of (dbbpy)Pt(tdt)·TENF. EHTB simulations on the (dbbpy)Pt(tdt)·TENF crystal structure yielded the total density of states (DOS) of the D/A stack shown in Figure 3 along with different projections

(6) Landrum, G. A.; Glassey, W. V. *YAeHMOP* (*version 3.0*). The YAeHMOP program is freely available on the web site: http://yaehmop.sourceforge.net/.

(7) (a) Payne, M. C.; Teter, M. P.; Allan, D. C.; Arias, T. A.; Joannopoulos, J. D. *Rev. Mod. Phys.* **1992**, *64*, 1045. (b) Brother, E. N.; Izmaylov, A. F.; Normand, J. O.Barone, V.; Scuseria, G. E. *J. Chem. Phys.* **2008**, *129*, 011102.

(8) See, for example, (a) Chai, S.-H.; Liu, C.-W. *J. Chem. Soc., Faraday Trans.* **1995**, *91*, 479. (b) Lopes, E. B.; Alves, H.; Ribera, E.; Mas-Torrent, M.; Auban-Senzier, P.; Canadell, E.; Henriques, R. T.; Almeida, M.; Molins, E.; Veciana, J.; Rovira, C.; Jerome, D. *Eur. Phys. J.* **2002**, *B29*, 27.

(9) (a) Kresse, G.; Hafner, J. *Phys. Rev. B* **1994**, *49*, 14251. (b) Kresse, G.; Furthmuller, J. *Comput. Mater. Sci.* **1996**, *6*, 15. (c) Kresse, G.; Furthmuller, J. *Phys. Rev. B* **1999**, *54*, 1758. Methfessel−Paxton smearing (width 0.2 eV) was used for these simulations: Methfessel, M.; Paxton, A. T. *Phys. Rev. B* **1989**, *40*, 3616.

(10) Kresse, G.; Joubert, D. *Phys. Rev.* **1999**, *B59*, 1758.

(11) Perdew, J. P.; Burke, K.; Ernzerhof, M. *Phys. Rev. Lett.* **1996**, *77*, 3865.

(12) Monkhorst, H. J.; Pack, J. D. *Phys. Rev. B* **1976**, *13*, 5188.

(13) Vanderbilt, D. *Phys. Rev. B* **1990**, *41*, 7892.

(14) Frisch, M. J.; Pople, J. A.; et al. *Gaussian 03, revision C.02*; Gaussian Inc., Wallingford, CT, 2004.

(15) Stevens, W. J.; Basch, H.; Krauss, M. *J. Chem. Phys.* **1984**, *81*, 6026.

(16) (a) Becke, A. D. *J. Chem. Phys.* **1993**, *98*, 1372. (b) Lee, C.; Yang, W.; Parr, R. G. *Phys. Rev.* **1998**, *B37*, 785.

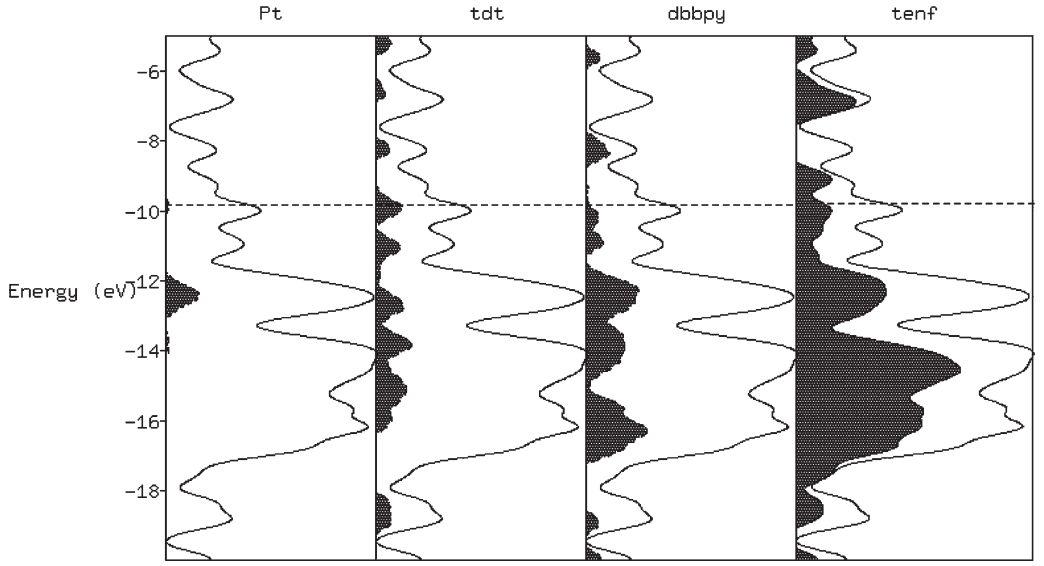

Figure 3. Plot of EHTB density of states of (dbbpy)Pt(tdt)·TENF. Solid curves indicate the total DOS. From left to right, the Pt, tdt, dbbpy, and TENF projections are given by the shaded areas that indicate their contributions to the total DOS. The horizontal dashed line corresponds to the Fermi level.

for the tdt, dbbpy, TENF, and Pt fragments that comprise the material of interest. The Fermi level lies in a region of high DOS at −9.95 eV. Therefore, (dbbpy)Pt(tdt)·TENF presents no band gap and it is predicted to be metallic according to the EHTB calculations. In the Fermi area a significant contribution from the π/π^* TENF band is indicated.

In Figure 3, we observe a small atomic Pt contribution near the Fermi level ∼−9.9 eV, while the major donor contribution in the conduction region is from tdt, consistent with our previous simulations and experiments for related mixed imine-thiolate d^8 complexes.[4b,c] The peak at ∼−12 eV corresponds to the four occupied Pt "d" orbitals of the formally Pt(II) complex. Just below the Fermi level of the crystalline D/A stack material, in the range of −10.1 to −12.0 eV, more so sulfur double-dispersed band was formed with nitrogen and sulfur lone pairs of dbbpy and tdt, respectively, mixed with a π_{TENF} component. The valence band thus possesses significant π character from the TENF acceptor. The conduction band is concentrated on the TENF moiety in π^* orbitals with some mixing of π^*_{tdt} and π^*_{dbppy} character. As a consequence of this interaction between organic and inorganic fragments, the valence and conduction bands are mainly situated on the organic ligands. It is somewhat surprising to see strong contribution from TENF in the valence band; this is likely due to significant interaction with the tdt primary donor moiety, consistent with the crystal structure (Figure 1).

From our DOS analysis, the interesting electronic properties[1] of (dbbpy)Pt(tdt)·TENF are consistent with the band constitution near the Fermi level, which are available to transfer electron density from the valence band to the low-energy conduction band (π^*) primarily on the TENF acceptor. Thus, we consider that interaction between donor and acceptor bands in the Fermi zone will influence drastically the valence/conduction bands in electron transfer and control conductive properties of these and related materials. Furthermore, it is supposed from the EHTB simulations that the close (∼3.5 Å) D:A distances in (dbbpy)Pt(tdt)·TENF are sufficient enough to allow charge sharing along the linear chains of molecules via charge transfer, as seen also in TTF-TCNQ materials.[1e] The EHTB computations further support the interpretation of the electrochemical data, which suggest that the reduction of the binary adduct is localized on the nitrofluorenone acceptor.[1c] Finally, charge transfer will greatly affect the acceptor molecule, given their significant contribution to the valence and conduction bands, a result consistent with other computational data and experimental IR spectra[1b] (vide infra).

2. EHTB Electronic Structure of [(dbbpy)Pt(tdt)]$_2$·TENF. This section focuses on the EHTB investigation of [(dbbpy)-Pt(tdt)]$_2$·TENF. The material presents the new stacking sequence DD/A. In Figure 4, we illustrate the DOS plots for the DD/A stacking. The material is predicted to exhibit metallic behavior, but with different band contributions. Interestingly, the Fermi level shifts to −9.55 eV (DD/A) from −9.95 eV (D/A) and the valence band becomes less dispersed in terms of the dbbpy contribution in this region for [(dbbpy)Pt(tdt)]$_2$·TENF (compare the window between −10 and −16 eV; Figures 3 and 4).

Figure 5 is a magnification of the DOS in the region of the greatest calculated Pt contribution for [(dbbpy)Pt(tdt)]$_{1,2}$·TENF below the valence band (∼−12 eV), which thus indicates that the Pt contribution for the DD/A (Figure 5, right side) material is less than that for the corresponding D/A material (Figure 5, left side). This is consistent with the crystal structure, which shows that the DD pairs are held primarily via tdt/bpy electrostatic interactions rather than via Pt···Pt interactions. Near the Fermi level, [(dbbpy)Pt(tdt)]$_2$·TENF (Figure 4) has more tdt/dbbpy character and less TENF character than in (dbbpy)Pt(tdt)·TENF (Figure 3). As shown by the EHTB calculations on [(dbbpy)Pt(tdt)]$_2$·TENF in Figure 4, the absence of platinum contribution and the ligand contributions in the Fermi area confirm the proposal[4b,c] of significant charge transfer of type LL′CT (ligand−ligand charge transfer) in such donor species. The interesting electronic properties of this DD/A material are thus consistent with the transfer of electron density from a valence band with ligand π character to a low-energy conduction band (π^*) primarily localized on the TENF acceptor.

In summary, analysis of the band structure of crystalline (dbbpy)Pt(tdt)·TENF and [(dbbpy)Pt(tdt)]$_2$·TENF,

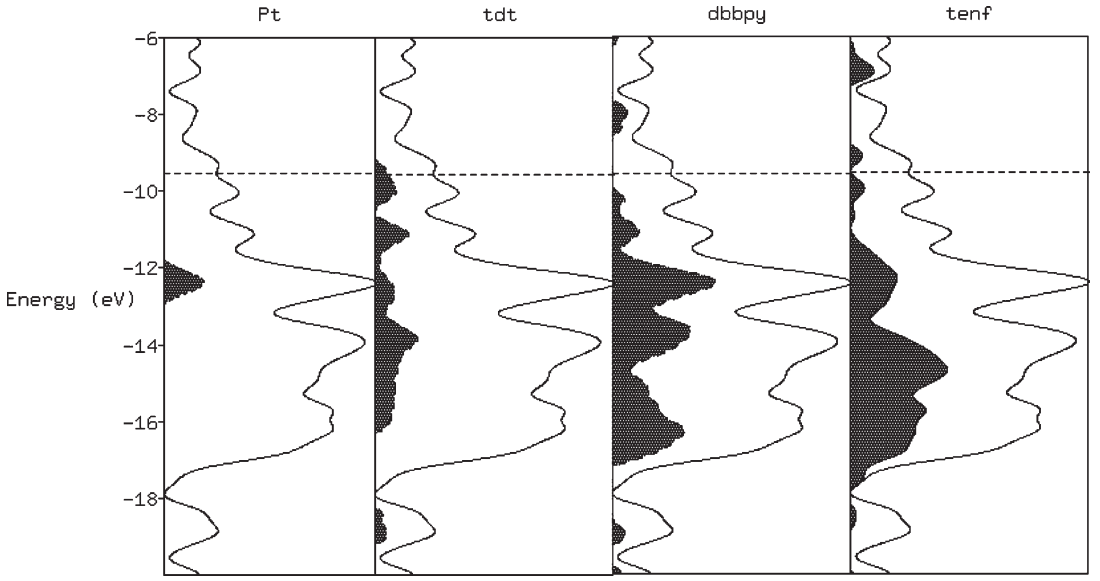

Figure 4. Plots of EHTB density of states of $[(dbbpy)Pt(tdt)]_2 \cdot TENF$. Solid curves indicate the total DOS. The projections that indicate the contributions to the total DOS are given by the shaded areas for (from left to right) Pt, tdt, dbbpy, and TENF. The horizontal dashed line corresponds to the Fermi level.

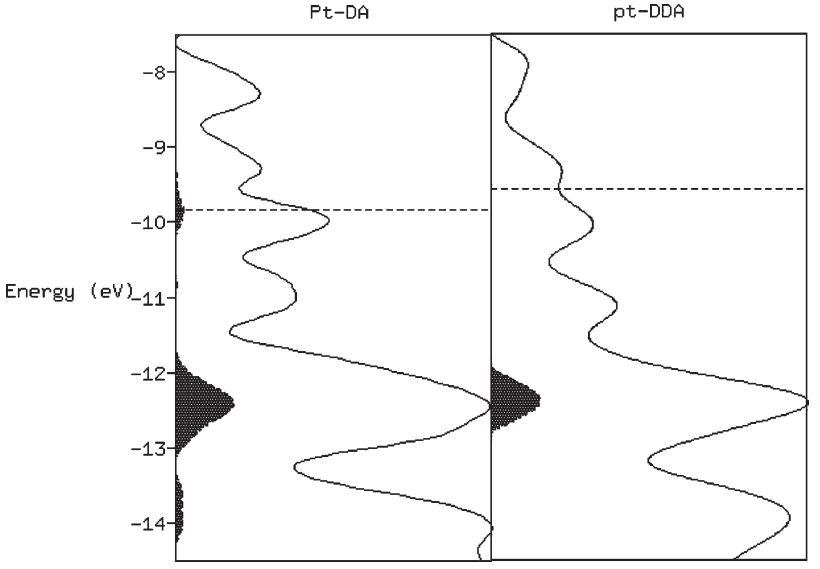

Figure 5. Magnification of the calculated Pt projection for $(dbbpy)Pt(tdt) \cdot TENF$ (left) versus $[(dbbpy)Pt(tdt)]_2 \cdot TENF$ (right).

demonstrates that both D/A (1:1) and DD/A (2:1) stacks display similar metallic behavior according to the band behavior near the Fermi level. We conclude from the EHTB calculations that the D/A stacks are electronically different in terms of charge transfer in the valence-conduction bands as compared to the DD/A stacks. Substantial changes of the first transition between D/A and DD/A are expected on the basis of the band constitution in the Fermi area (see Figure 5). In the first case, the D/A stack has a more significant metal contribution near the Fermi level than that in the DD/A stack. Therefore, the 1:1 stack material involves greater degree of MLCT charge transfer but LLCT is more pronounced and more probable in the 2:1 material. The greater dispersion of the valence bands of $(dbbpy)Pt(tdt) \cdot TENF$ as compared to $[(dbbpy)Pt(tdt)]_2 \cdot TENF$ suggests a greater ligand interaction via a charge transfer in 2:1 stacks. Finally, recall that the Fermi level in the DD/A stack is higher in energy than in the D/A material (−9.55 eV vs −9.95 eV, respectively).

Table 1. Experimental[1b,c] Lattice Parameters of $[(dbbpy)Pt(tdt)]_{1,2} \cdot TENF$ Used for Periodic DFT Simulations

param	$Pt(dbbpy)(tdt) \cdot TENF$	$[Pt(dbbpy)(tdt)]_2 \cdot TENF$
a (Å)	23.128(2)	11.257(2)
b (Å)	7.1640(6)	26.004(5)
c (Å)	25.474(2)	24.165(5)
α (deg)	90	90
β (deg)	109.19(10)	92.19(3)
γ (deg)	90	90

3. Plane-Wave Density Functional Calculations in D/A Stacking. Plane-wave DFT calculations were performed on $[(dbbpy)Pt(tdt)]_{1,2} \cdot TENF$ (D/A and DD/A) to provide a base of comparison with the faster, but more approximate, EHTB calculations. Note that for these plane-wave DFT simulations the *t*-Bu groups of dbbpy were replaced with hydrogen atoms to save computational effort and the lattice constants kept fixed at experimental values[1b,c] (Table 1).

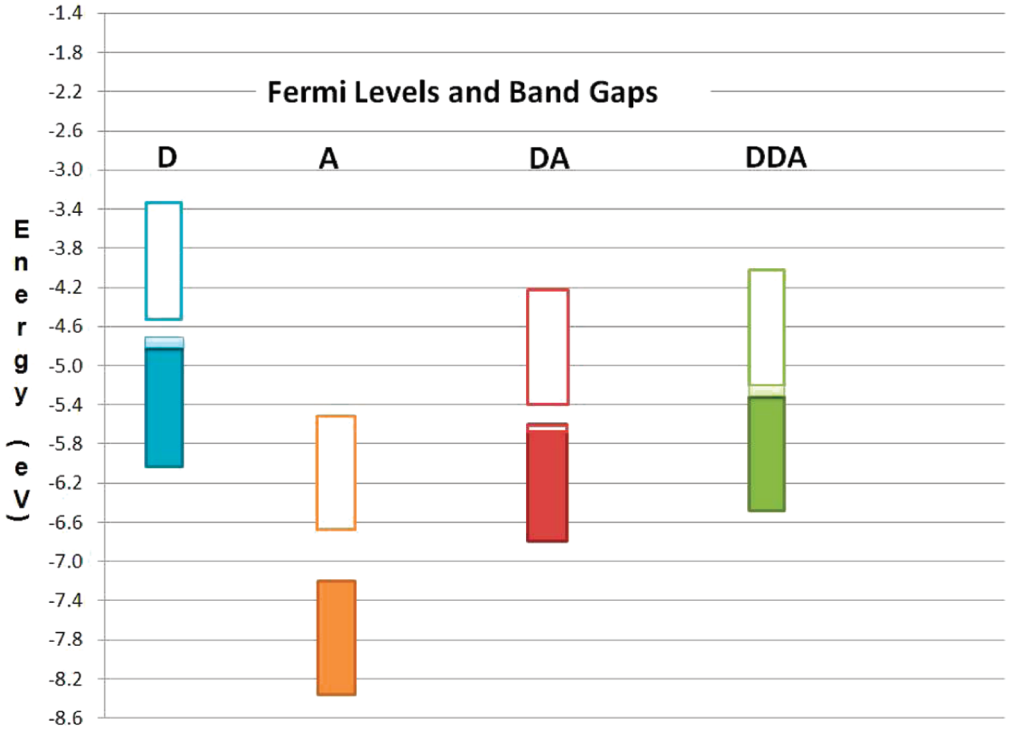

Figure 6. Schematic depiction of Fermi levels for D, A, D/A, and DD/A materials obtained via periodic plane-wave DFT simulations. The colored filled portions denote the valence band, and the empty portions denote the conduction band. Fermi energies for the materials investigated are as follows: D (−4.8 eV), A (−7.2 eV), D/A (−5.6 eV), and DD/A (−5.3 eV).

Heavy atoms were fixed at experimentally determined positions, while C−H bond lengths were standardized to 1.083 Å. VASP calculations were also carried out on the isolated D and A components using crystallographic coordinates for the D/A stack material. Given the expense of these systems and the large number of atoms (408 in the largest simulations) in the unit cell, neither lattice nor ionic relaxation was investigated.

The results obtained from the plane-wave DFT (PW-DFT) simulations of crystalline D, A, D/A, and DD/A are depicted in Figure 6. Three points are of interest with respect to the VASP simulations. First, the PW-DFT calculations support the EHTB supposition as to the increase (shifting) in the Fermi energy upon going from the D/A to the DD/A material. In the case of the PW-DFT calculations the increase is 0.3 eV (−5.6 eV → −5.3 eV) versus 0.4 eV from the EHTB calculations (−9.55 eV → −9.95 eV). Second, note the disposition of the Fermi level (−4.8 eV) for the isolated D molecules, while the A molecules show a considerably lower Fermi energy (−7.2 eV). This result is consistent with the flow of electrons from D to A, as suggested by the charge transfer model obtained from analysis of the EHTB simulations. One can deduce from Figure 6 that A and D present a much different electronic structure in isolation versus the ∼3.5 Å separation of their binary stacks. The interaction between D and A is noticeably substantial in D/A and DD/A stacks, which we propose from the calculations to be primarily via charge transfer. Third, the PW-DFT calculations suggest the DD/A material will be a better conductor, given that the Fermi level is located in a region of high DOS in terms of the filled bands. Overall, the PW-DFT and EHTB calculations show qualitatively similar features unless some difference has happened in D/A with some opening of band gap less than 0.1 eV, which is not too surprising for two different levels of theory.

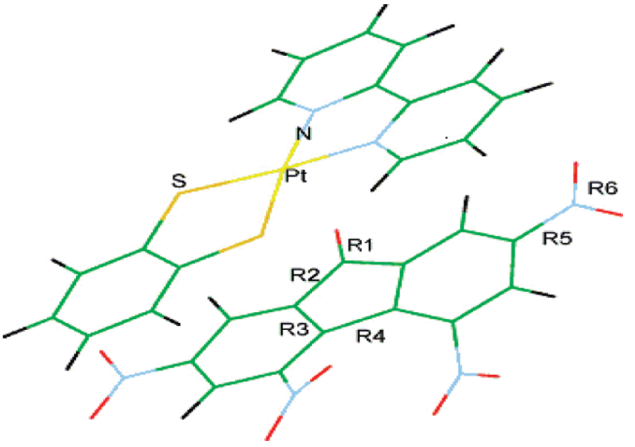

Figure 7. Molecular model of ((dbbpy)Pt(tdt)·TENF with important bonds labeled (see Table 2 for calculated values).

4. DFT Simulations of Molecular D/A and DD/A Models. Molecular calculations are carried out to further elucidate structural and electronic features of the D/A and DD/A stack materials. Also, molecular (Gaussian) DFT calculations remain more tractable than extended (plane-wave) DFT calculations. Hence, molecule-to-material mappings remain popular in both computational chemistry and computational material science, and thus it is of interest to compare/contrast such simulations.

In this part of the research, a molecular model is constructed, representing single DA and DDA links from a solid-state chain. All structures were optimized via DFT calculation (B3LYP/CEP-31G(d)) (see Figure 7 and Table 2). Note that test molecular calculations with the PBE functional (which was used in the VASP calculations) were

Table 2. Comparison of Experimental and Computed DFT Bond Distances (Å) in Isolated TENF (Left) and (dbbpy)Pt(tdt)·TENF (D/A and DD/A) Complexes (Right)[a]

					calcd		exptl	
metric	exptl TENF	calcd TENF	calcd $TENF^-$	calcd $TENF^{2-}$	D/A	DD/A	D/A	DD/A
R_1	1.49	1.49	1.50	1.50	1.50	1.50	1.50	1.50
R_2	1.48	1.50	1.50	1.50	1.50	1.51	1.51	1.52
R_3	1.41	1.41	1.46	1.48	1.43	1.44	1.40	1.43
R_4	1.49	1.49	1.47	1.42	1.50	1.49	1.51	1.50
R_5	1.47	1.48	1.46	1.42	1.48	1.48	1.49	1.47
R_6	1.21	1.23	1.30	1.32	1.29	1.29	1.24	1.28
Pt−N					2.08	2.07	2.07	2.07
Pt−S					2.35	2.36	2.30	2.36
					3.64[b]	3.70[b]	3.60[b]	3.67[b]

[a] Bond labels are given in Figure 7. Experimental X-ray data for TENF in D/A and DDA are given in the rightmost column, while isolated TENF data are shown in the second column. [b] Short interplanar distances corresponding to the closest platinum−carbon (on TENF) distance.

conducted to evaluate the impact of this choice; no significant differences upon calculated molecular properties were obtained. These molecular calculations were carried out on $[(dbbpy)Pt(tdt)]_{1,2}\cdot TENF$ and also on isolated TENF (neutral, anion, and dianion) to address the electronic and vibrational structure of these materials.[1c] Table 2 (column 2) gives computed bond lengths for TENF, and on the right side of Table 2 calculated and experimental data for $[(dbbpy)Pt(tdt)]_{1,2}\cdot TENF$ are presented.

B3LYP/CEP-31G(d) optimization was performed on D, A, D/A, and DD/A molecular models, and in each case, the geometry optimization was initiated from crystal structure geometries. For the molecular materials, the HOMO (corresponding to the Fermi level in periodic calculations) increases upon going from the D/A to DD/A model by 0.1 eV. This is similar in direction but less in magnitude than the Fermi level shift inferred from both the EHTB and PW-DFT calculations. The calculations indicate a limited degree of charge transfer (<0.03e) in the D/A and DD/A molecular models, reflecting a shortcoming of either the Mulliken population analysis scheme and/or DFT limitations in describing weak intermolecular interactions; since such interactions in DA and DDA units are cooperative, this was less of an issue in the PW-DFW periodic computations. Interestingly, the D−A interaction enthalpy in the D/A material is calculated to be −13.2 kcal/mol, but the overall interaction enthalpy is calculated to more than double for the DD/A material (−28.2 kcal/mol). This could suggest a cooperativity of interaction between the D units in the DD/A stacks to enhance the overall interaction among the various subunits.

Bond metrics may provide a measure of the degree of reduction of the TENF acceptor in (dbbpy)Pt(tdt)·TENF and $[(dbbpy)Pt(tdt)]_2\cdot TENF$. The two most sensitive bonds to TENF reduction (see columns 3−5 in Table 2) are those labeled R_3 and R_6; the latter is the average nitro NO bond length while the former is the bond where the five- and six-membered rings are fused together. In the D/A stack, calculated $R_3 = 1.43$ Å and $R_6 = 1.29$ Å versus 1.44 and 1.29 Å for R_3 and R_6 in the DD/A stack. Experimentally, $R_3 = 1.40$ and 1.43 Å for D/A and DD/A materials, respectively, while $R_6 = 1.24$ and 1.28 Å for the 1:1 and 2:1 materials, respectively. The resolution between the calculated D/A and DD/A bond lengths is not sufficient enough for us to confidently make any conclusions with regard to the reduction level of the TENF acceptor. Comparing the computed metric and experimental data (Table 2), we propose that the TENF oxidation state in the parent crystal structure is closer to $TENF^-$ than to $TENF^{2-}$. The existence of a reduced TENF species in either binary D/A or DD/A unit is unquestionable according to Table 2 data.

Conclusion

Tight-binding analyses of crystalline $[(dbbpy)Pt(tdt)]_{1,2}\cdot TENF$ and density functional calculations on molecular models are reported. Theoretical results give evidence of semimetallic behavior for the D/A material (gap <0.1 eV) and metallic behavior for DD/A. The valence-conduction band of EHTB solid-state calculations (dbbpy)Pt(tdt)·TENF is mainly localized on the π/π^* bands of TENF with a small mixing of Pt that facilitates charge transfer in the case of D/A stacking. Additionally, from EHTB calculations, the shape of the projected DOS on Pt atoms is found to be sensitive to the stacking level. A Mulliken population analysis is consistent with other pieces of evidence with respect to the charge transfer mechanism proposed experimentally. Meanwhile, the EHTB suggests substantial changes in the conduction properties upon modification of stacking D/A to DD/A, resulting in greater donor contribution and higher Fermi level. We note that dispersion and conduction band differences are more emphasized in DD/A than in D/A (see Figures 5 and 6) in terms of charge transfer and interaction between metallic and organic fragments, indicating a substantial contribution from TENF and tdt in this transfer (vide supra). In addition, the EHTB results agree with the PW-DFT calculations, which suggest the DD/A material will be a better conductor than D/A with filled bands and the Fermi level is located in a region of high DOS.

Acknowledgment. H.R. acknowledges UNT Chemistry and CASCaM for support. M.A.O. and T.R.C. the National Science Foundation (CHE-0911690) and the Texas Advanced Research Program (009741-0089-2007) for support. Calculations employed the UNT computational chemistry resource, supported by the NSF through grant CHE-0741936. Partial support by the Welch Foundation (Grant B-1542 to M.A.O.) and NSF (Grant CHE-0701247 to T.R.C.) is acknowledged. This research was also supported in part by a grant of supercomputer time to T.R.C. by the National Science Foundation through TeraGrid resources provided by the NCSA.